Corrosion behaviour of X100 pipeline steel under a salty droplet covered by simulated diluted bitumen

Hongxing Liang [a], Jing Liu [a], Akram Alfantazi [b], Edouard Asselin [a]

[a] Department of Materials Engineering, The University of British Columbia, Vancouver, BC, Canada

[b] Department of Chemical Engineering, The Petroleum Institute, Abu Dhabi, United Arab Emirates

Abstract

A NaCl-containing water droplet covered by simulated diluted bitumen was used to mimic the internal corrosion scenario that pipelines transporting diluted bitumen may encounter. The NaCl-containing droplet on the X100 pipeline steel shrank to a smaller droplet under the action of the simulated diluted bitumen. Hematite and lepidocrocite were identified in the corrosion products formed in the shrunken droplet. The dissolution of X100 pipeline steel primarily occurred at the edge of the central ring of the shrunken droplet. The corrosion attack morphology seen under these conditions is quite different from that of previous investigations for salty droplets in open air. The results point to a new mechanism of internal corrosion possibly appearing in diluted bitumen pipelines.

1 Introduction

Bitumen production is forecasted to grow rapidly over the next decade [1]. It was reported that the production of bitumen will increase up to 3.95 million barrels per day (b/d) by 2030 from 2.16 million b/d in 2014 [1]. These large amounts of bitumen are primarily transported in pipelines from the extraction sites to the refineries. Bitumen must be diluted in order to be pumped through a pipeline effectively, because bitumen itself is too thick to flow [2]. The content of basic sediments and water in diluted bitumen (dilbit) pipelines is less than 0.5% (vol.) [3]. The trace amounts of water that cannot be completely removed by current technologies exists as dispersed droplets in dilbit pipelines. Some water droplets become stagnant in dead legs and in low spots of dilbit pipelines, where the flow rate is low or static [4]. If stagnant droplets accumulate and persist on the pipeline surface, internal corrosion of the pipeline steel may occur.

As far as we are aware, the internal corrosion behaviour (including the corrosion attack morphology and type of corrosion products) has not been studied for pipeline steel under a droplet in dilbit pipelining conditions. Han et al. [3] investigated the electrochemical corrosion behaviour of pipeline steel beneath a salty droplet covered by paraffin oil at room temperature; however, they did not study the following two aspects. Firstly, because dilbit forms a stronger bond with metal surfaces than paraffin oil, dilbit has a higher tendency to adsorb on metal surfaces, which can significantly reduce the contact area between the droplet and steel [5]. Secondly, the types of corrosion products that form at room temperature are different from those that form at the operating temperature of dilbit pipelines (60°C). A high temperature (60°C) favors

hematite production, whereas room temperature favors the production of lepidocrocite and goethite [6].

2 Experimental

2.1 Materials

The material investigated was X100 pipeline steel (composition: C 0.1; Cr 0.016; Nb 0.043; V 0.003; Ni 0.13; Mo 0.19; Ti 0.02; Cu 0.25; Al 0.02; Mn 1.66 [wt%], Fe balance). The X100 was cut into 10 x 10 mm square pieces with a thickness of 6 mm. Each specimen was then ground with silicon carbide papers (120, 320, 600 and 1200 grit), followed by ultrasonic rinsing using reagent-grade alcohol.

2.2 Droplet Corrosion Treatment

Bitumen was diluted with paraffin oil (VWR analytical grade) to simulate dilbit with a 30:70 paraffin oil to bitumen volume ratio. The simulated dilbit and the 0.1 $\mathrm{gL^{-1}}$ sodium chloride (NaCl, Cryst./Certified ACS) solution were poured into different jacketed cells with an inner diameter of 70 mm and a height of 90 mm. These cells were preheated to 60 ± 1°C by circulating hot water through the jackets. A specimen was then placed in the third jacketed cell. A droplet of $10\mu\mathrm{L}$, directly taken from the 0.1 $\mathrm{gL^{-1}}$ NaCl solution (to simulate the droplets possibly formed in dilbit pipelines [3]) was placed on the specimen surface by a micropipette. Afterwards, the simulated dilbit preheated to $60℃$ was used to completely cover the droplet with a thickness of 40 mm. The temperature was controlled at 60 ± 1°C. After 24 h, the specimen surface was cleaned using toluene ($\mathrm{C_6H_5CH_3}$, VWR) to remove simulated dilbit on the specimen.

2.3 Corrosion Product Analysis

SEM images were taken using a field emission SEM (Zeiss Rigma) coupled with Energy dispersive X-ray spectrometry (EDS). The accelerating voltage during SEM measurements was 20 kV. The three-dimensional corrosion morphology under the corrosion products was measured by a surface profilometer (Tencor P10).

The corrosion products were tested with a Bruker GADDS micro-diffractometer with a collimator of 100μm and a radiation of Cu Kα. The measurement time was 1200 s. Conventional X-ray diffraction (XRD) patterns were obtained from the two-dimensional diffraction data by Chi integration around the intersected Debye cones. Then MDI Jade software equipped with the data base PDF-2 (2004) was used to analyze the conventional XRD patterns. Raman spectroscopy measurement was performed on a LabRam HR (by Horiba Scientific) with the LabSpec 6 software. For the excitation, a He-Cd 441.6 nm laser was employed.

3 Results and Discussion

Fig. 1(a) shows an SEM image of the corrosion products of the specimen beneath a NaCl-containing droplet covered by simulated dilbit for 24 h. The outermost ring approximately indicates the initial diameter (4.5 mm) of the droplet on the specimen surface. When the droplet was covered by simulated dilbit, the droplet shrank from the outermost ring to a smaller ring (Fig. 1(a)). A heterogeneous distribution of corrosion products can be seen across the entire area under the shrunken droplet. The central region of the shrunken droplet shows more corrosion products. It appears that, initially,

pits formed in the center of the shrunken droplet and the Fe^{2+} concentration in the center of the shrunken droplet reached a sufficient level to cause precipitation [7]. After the removal of the corrosion products (Fig. 1(b)), most of the corrosion appeared to occur at the edge of the central ring. The EDS mapping of Fe, C, O and Cl for Fig. 1(a) and (b) are given in the right part of Fig. 1. Cl accumulated around the edge of the central ring of the corrosion products. The Cl^- would be transported, in proportion to the Fe^{2+} generated by the anodic reaction $(Fe \rightarrow Fe^{2+} + 2e^-)$, to the edge of the central ring by electrophoresis [8].

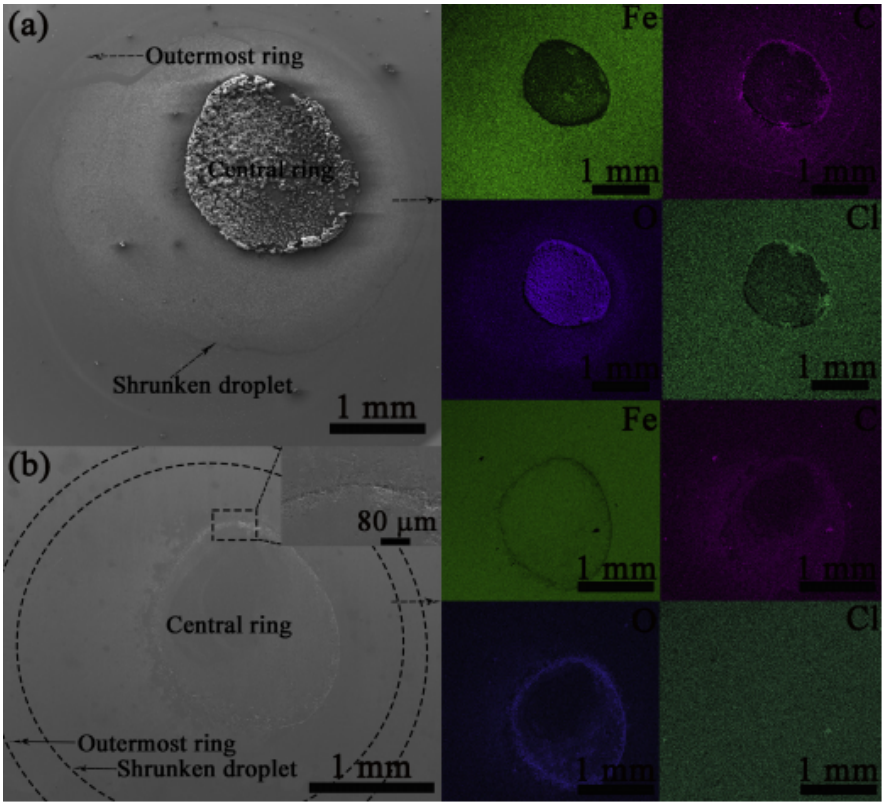

Fig. 1. SEM images (left) and EDS elemental mapping (right) for the surface morphology before (a) and after (b) the corrosion products were removed. The inserted SEM image in Fig. 1 (b) presents the high magnification morphology of the region in Fig. 1 (b).

The crystal structures in the corrosion products were characterized by SEM, Raman spectroscopy and micro-XRD. The microstructures in Fig. 2(a) are flower-like with a lamellar morphology, and they are assigned to lepidocrocite $(\gamma - \mathrm{FeOOH})$ [9]. The microspheres shown in Fig. 2(b) correspond to hematite $(\gamma - \mathrm{Fe_2O_3})$ [10]. The Raman spectrum (Fig. 2(c)) presents two peaks at 527 and 648 $\mathrm{cm^{-1}}$, which indicate lepidocrocite [9]. The peaks at 223, 292, 412, 496 and 610 $\mathrm{cm^{-1}}$ reveal the presence of hematite [9]. The micro-XRD plots in Fig. 2(d) suggest that the corrosion products are $(\gamma - \mathrm{FeOOH})$ and $(\gamma - \mathrm{Fe_2O_3})$ [11].

Pits may be initiated within the central ring, and the anodic dissolution occurs in the pits [12,13]. The cathodic reaction $(\mathrm{H_2O} + \frac{1}{2}\mathrm{O_2} + 2\mathrm{e^-} \rightarrow 2\mathrm{OH^-})$ proceeded at other regions of the shrunken droplet. The $\mathrm{Fe^{2+}}$ generated at pits diffused outwards, while the $\mathrm{OH^-}$ generated by cathodic reaction diffused inwards. Then the $\mathrm{Fe(OH)_2}$ was formed by $\mathrm{Fe^{2+}} + 2\mathrm{H_2O} \rightarrow \mathrm{Fe(OH)_2} + 2\mathrm{H^+}$ [12]. Therefore, an intermediate zone that presents relatively more corrosion products formed at the edge of the central ring. Since $\mathrm{Fe(OH)_2}$ is not stable it would further react to form lepidocrocite $(2\mathrm{Fe(OH)_2} + \frac{1}{2}\mathrm{O_2} = 2\mathrm{FeOOH} + \mathrm{H_2O})$ as well as hematite $(2\mathrm{FeOOH} = \mathrm{Fe_2O_3} + \mathrm{H_2O})$ [14].

According to the classic Evans model for droplet corrosion in open air, the anodic attack appears in the center of the droplet with the cathodic reaction occurring at the edge of the droplet due to the locally higher oxygen content [12,15]. However, the presence of simulated dilbit limits the oxygen supply [16]. Consequently, the Evans' theory is not applicable to the droplet corrosion of this study. Fig. 3 presents the three-dimensional corrosion morphology of the central ring in Fig. 1(b). Deep corrosion pits distribute along

the edge of the central ring. As the corrosion proceeded in the droplet covered by simulated dilbit, the oxygen in the shrunken droplet was consumed by the cathodic reaction and it may not have been sufficient to sustain the anodic dissolution in the pits [8].

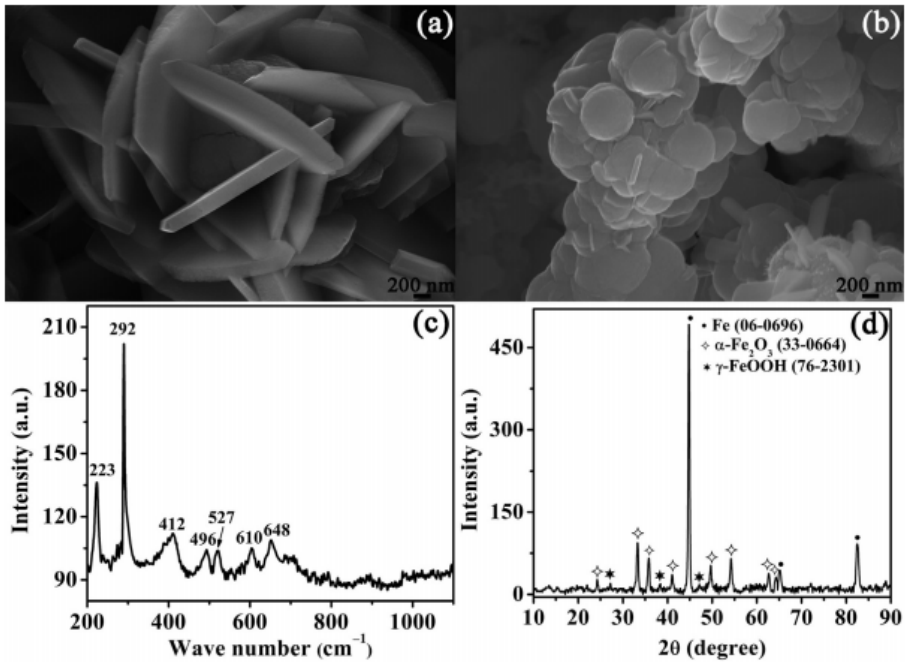

Fig. 2. SEM images (a and b), Raman spectrum (c) and micro-XRD (d) showing the crystal structures in the corrosion products

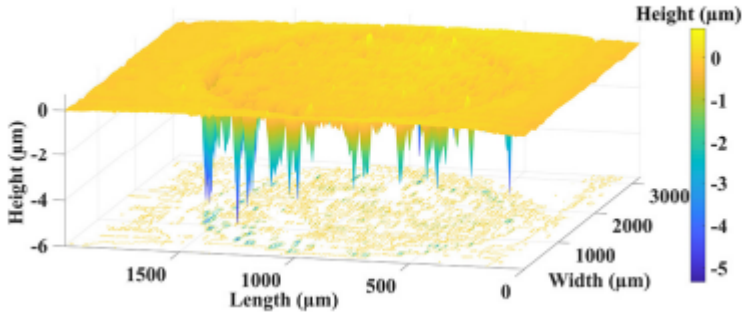

Fig. 3. Three-dimensional morphology of the corrosion attack under the corrosion products.

There were more corrosion products at the edge of the central ring than at other parts under the shrunken droplet (Fig. 1(a)). In the absence of oxygen, the reduction of the corrosion products at the edge of the central ring could have accepted electrons from the iron matrix, which would have accelerated the anodic dissolution of the iron matrix along the edge of the central ring [17]. The accumulation of Cl^- (Fig. 1(a)) would further accelerate the anodic dissolution at the edge of the central ring [8].

4 Conclusions

The droplet on the surface of pipeline steel can shrink through the action of simulated dilbit; and a heterogeneous distribution of corrosion products can be seen across the entire area under the shrunken droplet with the central part showing more corrosion products. Hematite and lepidocrocite were identified in the corrosion products. Most of the dissolution of X100 pipeline steel occurred at the edge of the central ring due to Cl^- accumulation and the reduction of the corrosion products at the edge of the central ring.

Acknowledgements

The financial support from the Natural Sciences and Engineering Research Council of Canada (NSERC) is greatly acknowledged. The corresponding author wishes to thank the Canada-China Scholarship Council for financial support of his doctoral studies.

Appendix A. Supplementary data

Supplementary data associated with this article can be found, in the online version, at https://doi.org/10.1016/j.matlet.2018.03.168.

References

[1] J.M. McKellar, S. Sleep, J.A. Bergerson, H.L. MacLean, Energy Policy 100 (2017) 162–169.

[2] J. Wu, T. Dabros, Energy Fuels 26 (2) (2012) 1002–1008.

[3] D. Han, R. Jiang, Y. Cheng, Electrochim. Acta 114 (2013) 403–408.

[4] I. Cole, D. Marney, Corros. Sci. 56 (2012) 5–16.

[5] H. Guan, S. Liu, Y. Duan, J. Cheng, Cem. Concr. Compos. 28 (5) (2006) 468–474.

[6] H. Liu, P. Li, M. Zhu, Y. Wei, Y. Sun, J. Solid State Chem. 180 (7) (2007) 2121–2128.

[7] V. Soulié, F. Lequien, F. Ferreira-Gomes, G. Moine, D. Feron, P. Prene, H. Moehwald, T. Zemb, H. Riegler, Mater. Corros. 68 (9) (2017) 927–934.

[8] T. Kamimura, K. Kashima, K. Sugae, H. Miyuki, T. Kudo, Corros. Sci. 62 (2012) 34–41.

[9] M. Morcillo, B. Chico, J. Alcántara, I. Díaz, R. Wolthuis, D. de la Fuente, J. Electrochem. Soc. 163 (2016) 426–439.

[10] Z. Li, X. Lai, H. Wang, D. Mao, C. Xing, D. Wang, Nanotechnology 20 (2009) 245603.

[11] N. Nava, E. Sosa, J. Alamilla, C. Knigth, A. Contreras, Corros. Sci. 51 (11) (2009)

2652–2656.

[12] R. Jiang, Y. Cheng, Electrochem. Commun. 35 (2013) 8–11.

[13] C. Yu, X. Gao, H. Wang, Mater. Lett. 209 (2017) 459–462.

[14] S. Li, L. Hihara, Electrochem. Commun. 18 (2012) 48–50.

[15] U.R. Evans, The Corrosion and the Oxidation of Metals, St. Martins Press, New York, 1960.

[16] D. Langevin, Adv. Colloid Interface Sci. 88 (2000) 209–222.

[17] T. Kamimura, M. Stratmann, Corros. Sci. 43 (3) (2001) 429–447.